Annual Symposium of the Hellenic Nuclear Physics Society

Τόμ. 1 (2025)

ANP2024 Special Volume

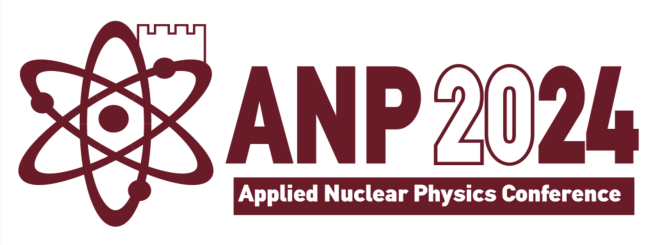

Modulating the electronic properties of Ag/Au implanted 2D chalcogenide layer on polymers

Romana Miksova, Giovanni Ceccio, Josef Novák, Anna Macková

doi: 10.12681/hnpsanp.8158

Βιβλιογραφική αναφορά:

Miksova, R., Ceccio, G., Novák, J., & Macková, A. (2025). Modulating the electronic properties of Ag/Au implanted 2D chalcogenide layer on polymers. *Annual Symposium of the Hellenic Nuclear Physics Society*, *1*(S01), 21–25. https://doi.org/10.12681/hnpsanp.8158

Modulating the electronic properties of Ag/Au implanted 2D chalcogenide layer on polymers

Romana Mikšová[1,*], Giovanni Ceccio[1], Josef Novák[1], Anna Macková[1,2]

[1] *Nuclear Physics Institute CAS, 250 68 Rez, Czech Republic*
[2] *Department of Physics, Faculty of Science, Jan Evangelista Purkyně University in Ústí nad Labem, 400 96 Ústí nad Labem, Czech Republic*

Abstract The unique properties enable molybdenum disulfide (MoS_2) exhibit great potential applications in the fields of electronic and optoelectronic devices. MoS_2 is a typical two-dimensional (2D) layered material shows low band gap. MoS_2 was developed on polyethylene terephthalate (PET) substrate for the construction of flexible devices with Ion beam sputtering (IBS). These MoS_2/PET composites were enriched with Ag and Au using ion beam implantation with energy up to 1.8 MeV and ion fluences in the range of 5×10^{14} to 5×10^{15} cm^{-2}. The implantation energy was chosen according to the SRIM simulation program to achieve the required depth for both ion species. Thickness of the MoS_2 layer as well as Ag and Au depth profiles were examined using Rutherford backscattering method (RBS). Surface morphology before and after ion beam implantation was checked using Scanning electron microscopy (SEM). The electrical properties of prepared structures were characterized by 2-point configuration. Ion implantation has been shown to decrease sheet resistance.

Keywords Molybdenum Disulfide, Ion Beam Sputtering, Ion Beam Implantation

INTRODUCTION

Graphene-like two-dimensional (2D) materials, such as molybdenum disulfide (MoS_2), hold great potential for applications in electronics, optoelectronics, electrocatalytic water splitting, and lithium-ion battery anodes [1–3]. MoS_2 has a tunable band gap, enhancing its suitability for advanced technologies. Its band gap depends on the number of monolayers: bulk MoS_2, an indirect-gap semiconductor (1.29 eV), consists of van der Waals-bonded S-Mo-S units [4], while monolayer MoS_2 transitions to a direct band gap of 1.8 eV. Tensile strain further modifies the band gap, potentially inducing a semiconductor-to-metal transition [5]. Polymers are widely used in microelectronics, biomaterials, and nanocomposites due to their strength, corrosion resistance, recyclability, and low cost [6]. Polyethylene terephthalate (PET), a thermoplastic polymer with good mechanical properties from its aromatic ring structure, has a wide band gap (3.8–4.3 eV), making it non-conductive [7]. However, its conductivity can be enhanced by metal doping. Our previous studies explored improving optical and electrical properties through ion beam implantation of metals into polymers or MoS_2 [9,10]. Ion implantation is a fundamental technique in semiconductor technology, allowing precise modification of material properties by introducing dopants or defects in a controlled manner. By adjusting ion beam energies, this method enables the synthesis of spatially non-uniform integrated materials with tailored electrical, optical, and mechanical characteristics [1]. It plays a crucial role in the fabrication of transistors, quantum devices, and optoelectronic components, facilitating advancements in miniaturization and performance optimization. Additionally, ion implantation offers high reproducibility and depth control, making it indispensable for modern microelectronics, advanced materials research, and emerging applications such as nanotechnology and quantum computing.

Our experiment primarily focuses on the implantation of MoS_2/PET structures with Au and Ag ions at energies of 1.8 MeV and 0.9 MeV, respectively. A combination of analytical techniques was employed to monitor structural modifications, hydrogen adsorption, and changes in electrical properties

* Corresponding author email: miksova@ujf.cas.cz

as a function of implantation fluence. The selected energies ensure ion penetration into the PET material while enabling analysis via the RBS method. Ion ranges were carefully adjusted to achieve similar implantation depths with a slight offset, resulting in a quasi-sandwich structure.

EXPERIMENTAL DETAILS

MoS_2 was deposited on 50 µm PET via ion beam sputtering (IBS) using a Low Energy Ion Facility (LEIF) system within CANAM [11]. Ar^+ ions (20 keV, ≈1 mA) sputtered a MoS_2 target (50 mm × 3 mm, 99.9% Porexi s.r.o.). The ion beam, focused on a ≈1 cm² area, struck the target at a 45° inclination, with a 10 cm target-substrate distance. A shutter prevented unwanted deposition during target cleaning. Ion implantation was performed with Ag (0.9 MeV) and Au (1.8 MeV) ions at fluences of 5×10^{14} - 5×10^{15} cm^{-2} (for each ion), with energies determined via SRIM-2013 simulations [12]. The ion beam was scanned for uniform distribution, and a turbomolecular pumping system maintained a pressure $<6\times10^{-5}$ Pa. A high-vacuum load-lock system minimized contamination, with 24-hour pre-experiment pumping.

Elemental concentration and thickness were analyzed using Rutherford Backscattering Spectrometry (RBS) with 2 MeV He^+ ions and Elastic Recoil Detection Analysis (ERDA) with 2.5 MeV He^+ ions for hydrogen detection. RBS used an ORTEC ULTRA-series detector (170° backscattering, Cornell geometry), while ERDA employed a Canberra PIPS detector with a 12 µm Mylar foil at a 30° angle (IBM geometry). Measurements were conducted at low current to prevent damage, with data analyzed using SIMNRA 7.03 [13].

Scanning electron microscopy (SEM) was used to analyze the surface morphology of pristine and irradiated MoS_2, with images captured using a Hitachi TM4000Plus operating at 5 kV in top-view mode. The sample was mounted on carbon conductive tape for imaging. Additionally, energy-dispersive X-ray spectroscopy (EDS) elemental mapping was performed to analyze the surface composition of MoS_2.

The electrical properties of the prepared structures were characterized using a two-point measurement with a Keithley 6317B electrometer. To facilitate these measurements, two gold (Au) contacts (50 nm thick, 10 mm long, and separated by a 1 mm gap) were deposited on the membrane surface, ensuring reliable detection of resistivity changes.

RESULTS AND DISCUSSION

SRIM simulations provided preliminary data on implanted ion depth distribution, electronic and nuclear stopping interplay, and Mo/S vacancy depth profiles in irradiated MoS_2. Simulations (Fig. 1) show that nuclear stopping dominates for Au and Ag ions, causing bond rupture and atom displacement. SRIM-projected ion ranges are $R_p = (463 \pm 121)$ nm for Ag and $R_p = (511 \pm 111)$ nm for Au. Simulated vacancy depth profiles (not shown) indicate that Au ions create ~2× more vacancies than Ag ions. For Mo and S vacancy profiles we used displacement energies, 5 eV for S, 31.7 eV for Mo [10].

RBS was used to control the sample stoichiometry and possible sulphur depletion. It must be emphasized, RBS was employed to monitor sample stoichiometry and assess potential sulfur depletion. It is important to note that the depth resolution of RBS for light elements, including sulfur, is limited to approximately 10 nm, with an analytical depth of about 1 µm. As a result, RBS primarily provides insights into bulk elemental composition. To analyze surface composition, complementary techniques such as EDS must be utilized. Typical RBS spectra of both pristine and irradiated samples are shown in Fig. 2. No significant sulfur depletion was observed beyond several tens of nanometers, as evidenced by the sharp and unaltered sulfur leading edge in the RBS spectra for all samples. Minor variations in sulfur concentration, within 5 at.%, were detected, but these remain within the uncertainty range of the RBS method. ERDA measurement showed (not shown here) small decrease in hydrogen content (in

PET) depending on the increasing ion fluences, decrease was about 4 at.% for lowest ion fluence and for the highest ion fluence was about 7 at%.

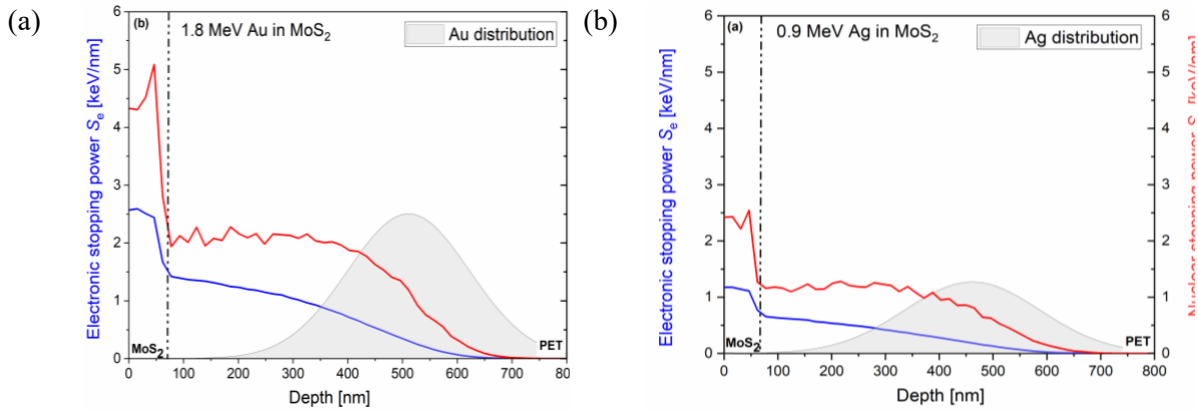

Figure 1. *Electronic and nuclear stopping depth profiles are presented together with ion concentration depth profiles (a) for energy 0.9 MeV Ag ions, and (b) for energy 1.8 MeV Au ions.*

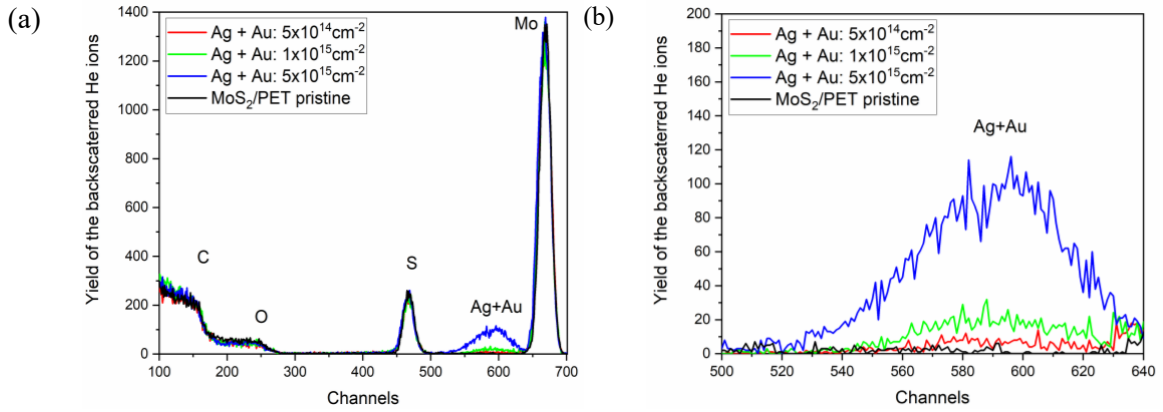

Figure 2. *(a) RBS specrum of MoS_2 irradiated by Ag and Au ions for different ion fluences; (b) Zoom in of the Ag and Au ions distribution.*

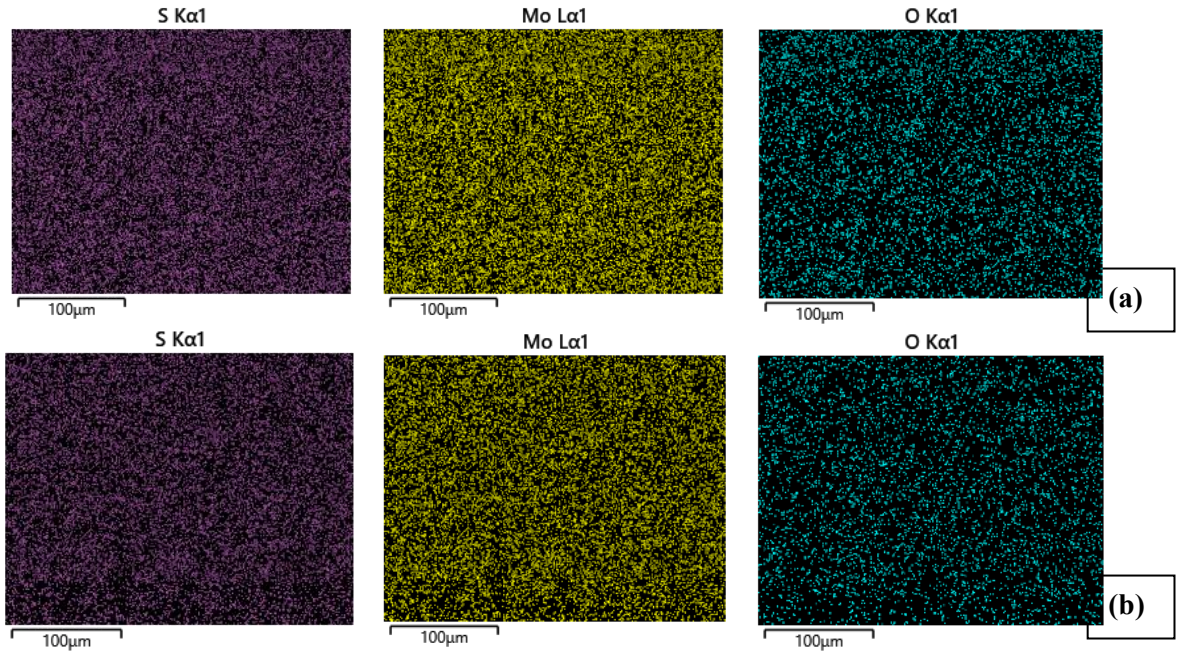

Figure 3. *Elemental composition using EDS for pristine (a) MoS_2/PET and for (b) MoS_2/PET implanted with the highest ion flunces.*

SEM analysis with EDS spectroscopy was used to monitor elemental composition changes. EDS images of MoS_2 (for S, Mo, and O, respectively) shown in Fig. 3a and 3b, depict the pristine sample and the sample implanted with Au and Ag ions at the highest fluences. This further confirmed the RBS results, indicating that sulfur loss and vacancy formation are minimal even under the highest irradiation fluence.

Using the two-point measurement method, we investigated the electrical resistivity of pristine and ion-irradiated MoS_2/PET samples. The pristine samples exhibited the lowest resistivity. The pristine samples exhibited the highest sheet resistivity.

We observed a decrease in sheet resistivity at the lowest ion fluences; however, as ion fluence increased, the sheet resistivity also exhibited an upward trend (see Fig. 4).

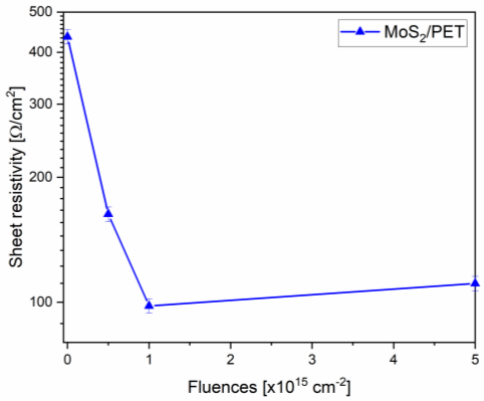

Figure 4. *Sheet resistivity measured as a function of the ion implantation fluence.*

At low ion fluences, defect-induced doping likely enhances carrier transport, leading to decreased sheet resistivity. However, at higher fluences, increasing structural damage and carrier scattering dominate, resulting in a rise in sheet resistivity due to disrupted charge transport pathways.

CONCLUSIONS

This study examined ion implantation effects on MoS_2/PET structures, focusing on structural, compositional, and electrical modifications by Ag and Au ions. MoS_2 was deposited via ion beam sputtering, followed by implantation at energies up to 1.8 MeV and fluences of 5×10^{14}–5×10^{15} cm^{-2}. SRIM simulations confirmed Au ions generate ≈2× more vacancies than Ag ions. RBS and ERDA analyses showed stable stoichiometry and a fluence-dependent hydrogen decrease. Electrical measurements revealed an initial resistivity drop, followed by an increase with fluence. This behavior could be attributed to changes in the material's microstructure and vacancy formation, which impact carrier mobility. These results demonstrate ion implantation as a viable method for tuning MoS_2/PET properties in flexible electronics.

Acknowledgments

The research has been carried out at the CANAM (Centre of Accelerators and Nuclear Analytical Methods) infrastructure LM 2015056. The scientific results were obtained with the support of the GACR Project No. 23-06702S and the University of J. E. Purkyne project UJEP-SGS-2023-53-007-2. The authors acknowledge the assistance provided by the Advanced Multiscale Materials for Key Enabling Technologies project, supported by the Ministry of Education, Youth, and Sports of the Czech Republic. Project No. CZ.02.01.01/00/22_008/0004558, Co-funded by the European Union.” – AMULET project.

References

[1] J. Luxa, et al., Appl. Mater. Today 14, 216 (2019); doi: 10.1016/j.surfin.2019.100357
[2] T. Stephenson, et al., Energy Env. Sci 7, 209 (2014); doi: 10.1039/C3EE42591F
[3] D. Vella, et al., 2D Mater. 4, 021005 (2017); doi: 10.1088/2053-1583/aa5784
[4] Th. Böker, et al., Phys. Rev. B 64, 235305 (2001); doi: 10.1103/PhysRevB.64.235305
[5] Q. Yue, et al., Phys. Lett. A 376, 1166 (2012); doi: 10.1016/j.physleta.2012.02.029
[6] Y.H.A. Fawzy, et a;, Surf. Rev. Lett. 25, 1850066 (2018); doi: 10.1142/S0218625X1850066X
[7] S. Brunner, et al., Surf. Coat. Technol. 200, 5908 (2006); doi: 10.1016/j.surfcoat.2005.09.011
[8] R.C. Ramola, et al., Phys. B Condens. Matter 404, 26 (2009); doi: 10.1016/j.physb.2008.09.033
[9] P. Malinsky, et al., EPJ Web Conf. 261, 02006 (2022); doi: 10.1051/epjconf/202226102006
[10] A. Macková, et al., Surf. Interfaces 17, 100357 (2019); doi: 10.1016/j.surfin.2019.100357
[11] A. Macková, et al., J. Tecl, Eur. Phys. J. Plus 136, 558 (2021); doi: 10.1140/epjp/s13360-021-01430-y
[12] J.F. Ziegler, et al., Nucl. Instrum. Meth, Phys. Res. B 268, 1818 (2010); doi: 10.1016/j.nimb.2010.02.091
[13] M. Mayer, in: AIP Conf. Proc., AIP, Denton, Texas (USA), 1999, pp. 541–544; doi: 10.1063/1.59188